

EFFICIENCY OF MARKETABLE DECONTAMINATION AGENT AND GRAPHENE OXIDE ON ^{99m}Tc AND ^{131}I SPILLAGES IN NUCLEAR MEDICINE DEPARTMENT

by

Mohammad Khairul Azhar Abdul RAZAB^{1*}, **Norazlina Mat NAWI**², **Rosidah SUNAIWI**¹,
An'amt Mohamed NOOR³, **Mohd Zahri Abdul AZIZ**⁴, **Fara Hana Mohd HADZUAN**¹,
Fathirah IBRAHIM¹, **Ahmad Thaufur KHAIZUL**^{1,2}, and **Nor Hakimin ABDULLAH**³

¹ Medical Radiation Programme, School of Health Sciences, University of Sains Malaysia, Kubang Kerian, Kelantan, Malaysia

² Department of Nuclear Medicine, Radiotherapy and Oncology, School of Medical Sciences, University of Sains Malaysia, Kubang Kerian, Kelantan, Malaysia

³ Advanced Materials Research Cluster, Faculty of Bioengineering and Technology, University of Malaysia Kelantan, Jeli, Kelantan, Malaysia

⁴ Oncological and Radiological Sciences Cluster, Advanced Medical and Dental Institute, University of Sains Malaysia, Bertam, Kepala Batas, Pulau Pinang, Malaysia

Scientific paper

<https://doi.org/10.2298/NTRP2202159R>

Dealing with open sources of radioactive substances in nuclear medicine is a daily task since contamination due to radioactive spills may happen frequently. Proper and safe decontamination management is a vital procedure. However, regular purchase of decontamination agents incurs high costs and might be toxic due to their chemical properties. The purpose of this study is to compare graphene oxide, which is an environmentally friendly carbon-based material and marketable decontamination agent, in decontaminating radioactive spillage. Samples of pure ^{99m}Tc and ^{131}I from the laboratory were spilled on a petri dish. The spill was immediately decontaminated with a marketable decontamination agent swab and varying concentrations of graphene oxide swab. The initial radioactivity of each swab containing ^{99m}Tc and ^{131}I was measured using a dose calibrator. The absorbance spectra of each sample were analysed using an ultraviolet-visible spectrophotometer. The morphology image of graphene oxide was observed under field emission scanning electron microscope. For decontamination using a marketable decontamination agent, the radioactivity of ^{131}I was slightly higher, whereas that of ^{99m}Tc was slightly lower than the high concentration of graphene oxide. The absorbance spectra of ^{99m}Tc and ^{131}I that had been decontaminated using graphene oxide were observed at a range of 200 nm to 250 nm due to the * transition.

Key words: nuclear medicine, radioactivity, ^{131}I , ^{99m}Tc , graphene oxide, spillage, decontamination

INTRODUCTION

A nuclear medicine department is one of the facilities that provide both diagnostic and therapeutic services for patients through the aid of radiopharmaceuticals. Specific radiopharmaceuticals are administered into a patient's body either orally or intravenously for diagnostic and/or therapeutic purposes [1]. The most common radiopharmaceuticals being used are ^{99m}Tc and ^{131}I [2, 3]. ^{99m}Tc is a radiotracer used for diagnostic purposes to image or measure the regional function and conditions of an organ in cases that include injuries, infections, tumours, heart disease, and thyroid abnormalities. In addition to that, it is also used to guide some cancer procedures.

* Corresponding author, e-mail: khairul.azhar@usm.my

^{99m}Tc is given to a patient by intravenous injection or orally depending on the organ that needs to be studied [4]. Meanwhile, ^{131}I is given to a patient in a single dose orally, in a capsule or liquid form. ^{131}I is used for therapeutic purposes to treat patients with thyroid diseases such as hyperthyroidism and thyroid cancer [1, 5].

The liquid form of both ^{99m}Tc and ^{131}I may involve a high risk of spillage, therefore, they need effective handling procedures. The routine elution, storage, and handling of ^{99m}Tc and ^{131}I need careful care to prevent any spills. If a minor or major spill happens, it will be identified as an emergency and coded. Thus, an adequate response plan is devised to prevent any radioactive adversity, especially for radiation workers. The plan is written and adopted as a standard operating procedure (SOP). Such plans are designed to apply to

all health workers, in every nuclear medicine department in response to a spill [6]. The SOP contains proper guidance to minimise the accident-related impact of a spill and the decontamination of radioactive material while supplementing the procedures stipulated by each institution.

Marketable decontamination agent (MDA) such as biodex medical systems has been widely used for the decontamination of radioactive spills in hospitals, laboratories, and reactor facilities as first-line general-purpose decontamination solutions [7]. The MDA removes radioactive particles from surfaces by sequestering metallic ions and then firmly suspending the contaminating particles, which allows these particles to be rinsed away with hard, soft or salt water [8]. However, the high cost of the commercial chemical agents, which is not environmentally friendly, leads to the proposal of other economical and sustainable resources. Graphene oxide (GO) seems to be an alternative of super absorbance in decontaminating radioactive spillage due to its availability and non-toxicity of these nanocomposites, with great potential in eco-friendly wastewater purification, due to high surface area and functional groups availability [9]. Decontamination studies using different chemical of MDA and GO in decontaminating the radionuclides has been conducted separately, and no significant comparison has been systematically documented. Thus, this study revealed the scientific correlations between the adsorption rate of selected MDA and GO for ^{99m}Tc and ^{131}I , for radionuclide decontamination efficiency.

METHODOLOGY

The experiment was performed at the Nuclear Medicine, Radiotherapy and Oncology Department, Hospital Universiti Sains Malaysia (HUSM). Four samples of ^{99m}Tc and another four samples of ^{131}I , with radioactivity of 1mCi ($1 \text{ Ci} = 3.7 \cdot 10^{10} \text{ s}^{-1}$) each, were prepared in syringes before being spilled slowly in the centre of methylene blue, on a petri dish to minimise the spread of the radionuclides spill. This step was carried out behind a protective lead glass of a workbench, in a hot laboratory. In this experiment, the background exposure rate mR h^{-1} ($1 \text{ R} = 258 \text{ C kg}^{-1}$) of the laboratory was measured using a pancake probe Geiger-Muller survey meter (Model 44-7, Ludlum, USA) for radiation safety. The ranges of the measurements were within 0-2 mR h^{-1} .

Synthesis of GO

GO was prepared according to simplified Hummer's method [10-12]. Initially, 3 g of graphite powder was mixed with 320 ml of H_2SO_4 solution and 80 ml of

H_3PO_4 solution with a ratio of 4:1. This was followed by slow addition of 18 g of KMnO_4 powder to obtain a mixture. The mixture was stirred for three days using a magnetic stirrer and poured onto a 500 ml ice cube along with 27 ml of H_2O_2 solution to stop the chemical reactions. Then, the mixture was centrifuged at 10000 rpm, washed three times with HCl and washed with distilled water until it reached pH 5. Finally, the GO solution was characterised using field scanning electron microscope (FESEM) (Quanta 450 FEG, FEI, USA) to validate the nanolayers of the GO sheets. Varying concentrations of GO (as shown in tab. 1) were prepared by diluting the GO with saline, using eq. (1)

$$M_1V_1 = M_2V_2 \quad (1)$$

where M_1 (mg ml^{-1}) is the initial concentration of GO with 3.3 mg ml^{-1} , used in this experiment, V_1 (ml) – the initial volume of GO, M_2 (mg ml^{-1}) – the concentration of GO after dilution, V_2 (ml) – the volume of GO after dilution.

Decontamination agent swabs with varying concentrations of GO were prepared. Adequate wads of cotton wool were drowned in glass containers containing varying concentrations of GO. Forceps were used to submerge the cotton wool for better absorption of the decontamination agent. This process assumed that the weight of cotton wools is negligible for GO concentration determination due to small volume measurements obtained (0.0001 mg).

The MDA concentration determination

A plain filter was weighed using an electronic beam balance which has the uncertainty 0.001 mg. Then, 1 ml of MDA was added to the filter paper and weighed. An MDA concentration of $1.1664 \text{ mg ml}^{-1}$ was determined using eq. (2). Decontamination agent swabs of MDA were prepared. Adequate cotton wool wads were drowned in glass containers containing MDA using forceps.

$$\text{MDA concentration (mg ml}^{-1}\text{)} = \frac{\text{Weight}_{\text{MDA + filter paper}} - \text{Weight}_{\text{filter paper}}}{1 \text{ ml MDA}} \quad (2)$$

Table 1. Ratio of concentration of GO

Concentration of GO [mg ml^{-1}]	Volume of GO [ml]	Volume of saline [ml]	Volume of GO after dilution [ml]	Measurement uncertainty for GO concentrations
1.0	1	3.30	4.30	0.1
2.0	1	1.65	2.65	0.1
3.0	1	1.10	2.10	0.1

Spillage decontamination

Using forceps, the prepared decontamination agent swabs were used to wipe the spill starting from the contaminated area, periphery moving towards the centre in a circular motion. This step was carried out behind the 10 mm protective lead glass on a workbench, in a hot laboratory. The activity (MBq) of radionuclides residue in the syringe was determined using a dose calibrator (Atomlab 500, Biodex Medical System, USA) to identify the exact level of activity that had been spilled on the petri dish. The reproducibility and accuracy of the measurements of the dose calibrator were within 5%. Then, four samples of cotton wool were obtained after decontamination: ^{99m}Tc:GO, ^{99m}Tc:MDA, ¹³¹I:GO, and ¹³¹I:MDA. The absorption spectra of each sample were determined using a UV-Visible spectrophotometer (Cary 100 Bio, Varian, USA). This spectrometer measured absorbance intensity from 100-700 nm wavelength with 5% uncertainty.

RESULTS AND DISCUSSION

Kinetic study

The radioactivity levels of ¹³¹I and ^{99m}Tc in the cotton wool, after decontamination, were obtained as in the initial activity using a dose calibrator and the time function (A_0 = initial activity: for ¹³¹I: $A_0/4 = 4$ days, $A_0/2 = 8$ days, $3A_0/4 = 12$ days and total decay = 16 days and for ^{99m}Tc: $A_0/4 = 3$ hours, $A_0/2 = 6$ hours, $3A_0/4 = 9$ hours and total decay = 12 hours), where the time was fixed based on the physical half-life of ¹³¹I (8 days) and ^{99m}Tc (6 hours). The decay graph was plotted for the radioactivity over time function for each sample of ¹³¹I and ^{99m}Tc. The kinetic study of the radionuclides adsorption in the cotton wool was calculated using the Beer-Lambert radioactive decay equation

$$\ln \frac{A}{A_0} = -\lambda t \quad (3)$$

where A is the radionuclide activity, A_0 – the initial radionuclide activity, λ – the decay constant, and t – decay time.

The extrapolation graph in fig. 1 shows the ¹³¹I and fig. 2 shows the ^{99m}Tc radioactivity after decontamination with MDA and different concentrations of GO over 16 days and six hours, respectively. The vertical axis in fig. 1 represents the activity of ¹³¹I in units of megabecquerel (MBq) on the first, fourth, eighth, 12th and 16th days, whereas the horizontal axis represents the days. The vertical axis in fig. 2 represents the activity of ^{99m}Tc in MBq units at the 0th, 3rd, and 6th hour, whereas the horizontal axis represents the hours. Overall, the graph pattern for the radioactivity of both ¹³¹I and ^{99m}Tc over time increased for both decontamination agents in the same way in which it decreased exponentially from the first day until the 16th day for ¹³¹I and from the 0th hour until the 6th hour for ^{99m}Tc as expected. The higher the concentration of GO, the higher the radioactivity of ¹³¹I measured (radionuclide adsorbability). This was due to the presence of more GO molecules in the higher concentrations of GO, which led to the high sorption rate of ¹³¹I. From the first day until the 16th day, the higher concentrations of GO molecules trapped ¹³¹I more efficiently. High GO concentrations demonstrated high sorption affinity for the most toxic radionuclides in various solutions whereby 2.0 mgml⁻¹ accelerate the ¹³¹I almost to 3.3% faster than 1.0 mg/mL at the initial stage (within 12 hours) of the decay process, as shown in fig. 1. Moreover, 3.0 mgml⁻¹ of GO and MDA show the same pattern and have equivalent adsorption rates for ¹³¹I from the 1st until the 4th stages of the decontamination process whereby the exponential decay lines overlapped each other. However, in detail, the activity of ¹³¹I with MDA was slightly higher than ¹³¹I with the maximum concentration of GO of 0.1% (yellow versus green

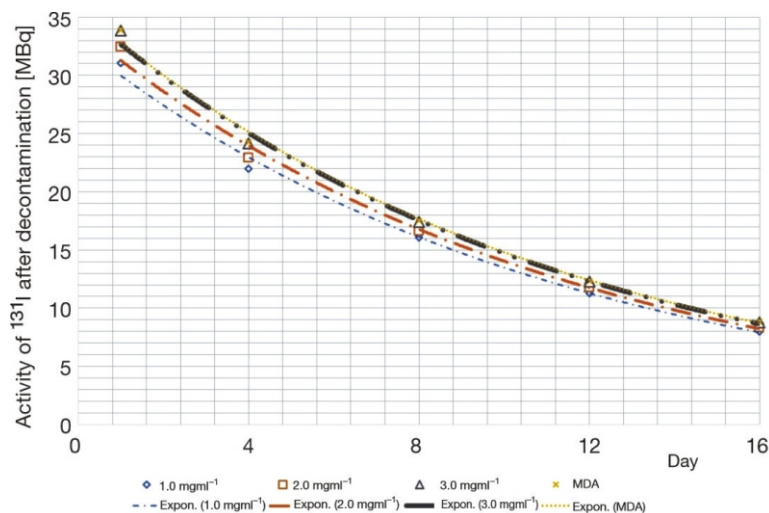


Figure 1. Activity of ¹³¹I after decontamination with MDA and different concentrations of GO over days

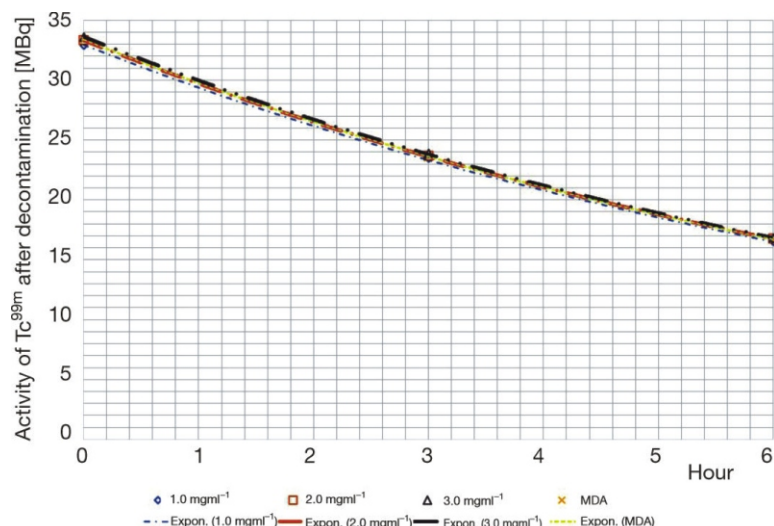


Figure 2. Activity of ^{99m}Tc after decontamination with MDA and different concentrations of GO over hours

lines in fig. 1). This might be due to active chemical interactions of MDA with ^{131}I that lead to better agglomeration mechanisms for a better adsorption process. A similar observation was obtained with ^{99m}Tc whereby the ^{99m}Tc activity increased as higher concentrations of GO were used, as shown in fig. 2. This was due to the more highly accessible surface areas and rich functional groups in higher concentrations of GO that are actively involved in agglomerating the radionuclide elements. The functional groups of GO could form strong surface complexes with cations and anions in radionuclides through electrostatic interaction. From the 0th hour until the 6th hour, the ^{99m}Tc activity with the maximum concentration of GO was slightly higher than the ^{99m}Tc activity with MDA by 0.1% (grey versus yellow lines in fig. 2). It seems that the MDA product performance was equivalent to 2.0 mgml⁻¹ of GO concentrations in adsorbing ^{99m}Tc radionuclides for the decontamination process. From the graph, 3.0

mgml⁻¹ is superior in accelerating the decontamination rate over MDA for ^{99m}Tc . This phenomenon might be due to the optimal volume of interactions between the high availability of functional groups in GO nanolayers with a high decay rate of ^{99m}Tc within short interactions time.

Absorbance spectra

Radionuclides decontaminated with MDA and a 2.0 mgml⁻¹ concentration of GO were chosen. The light absorption of chemicals in each sample, as mentioned earlier, was characterised using a UV-Visible spectrophotometer and the maximum absorption peaks were observed. The UV-visible spectra of ^{131}I :GO and ^{99m}Tc :GO are shown in fig. 3 and fig. 4, respectively, while the UV-visible spectra of ^{131}I :MDA and ^{99m}Tc :MDA are shown in fig. 5 and fig. 6, respectively.

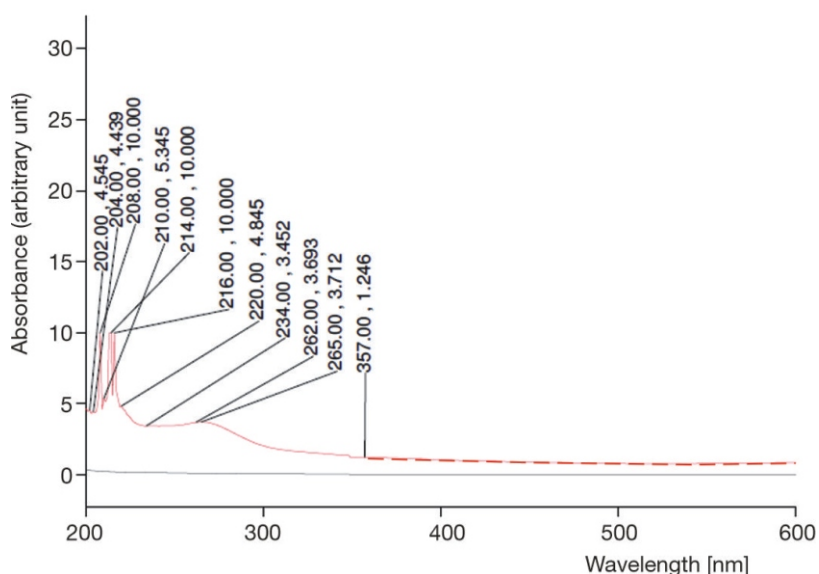


Figure 3. The UV-visible spectra of ^{131}I :GO

Figure 4. The UV-visible spectra of $^{99m}\text{Tc:GO}$

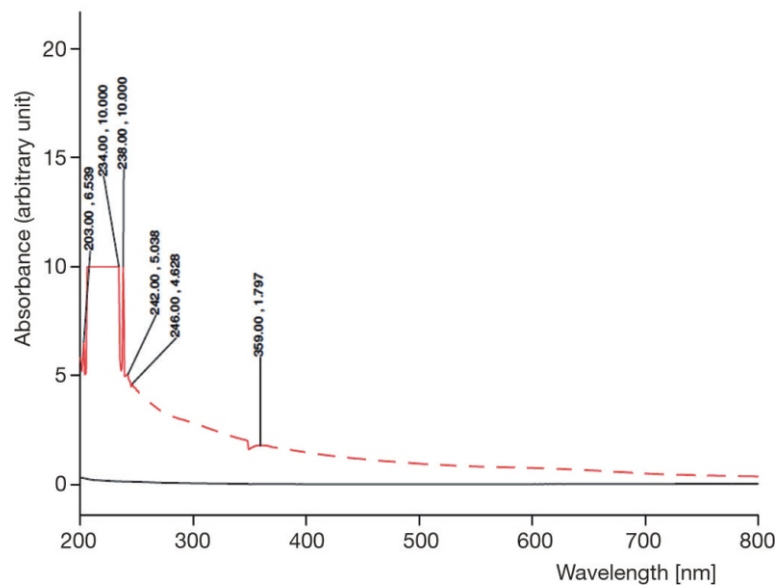


Figure 5. The UV-visible spectra of $^{131}\text{I:MDA}$

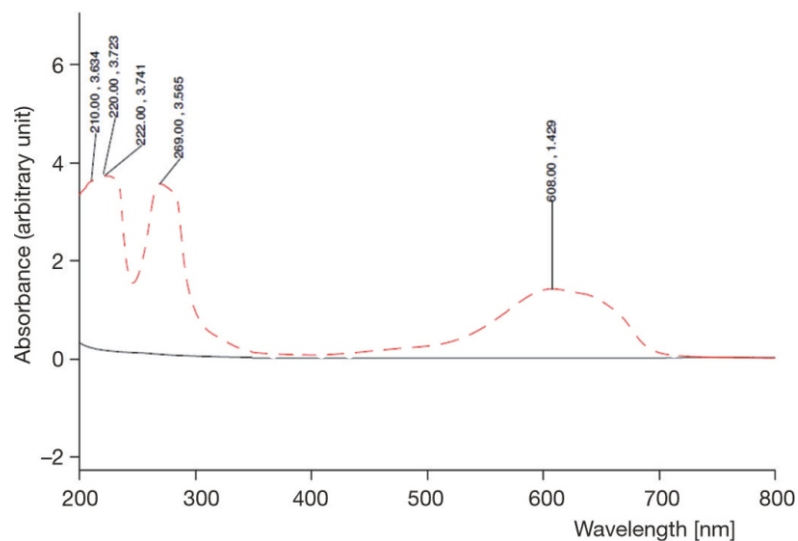
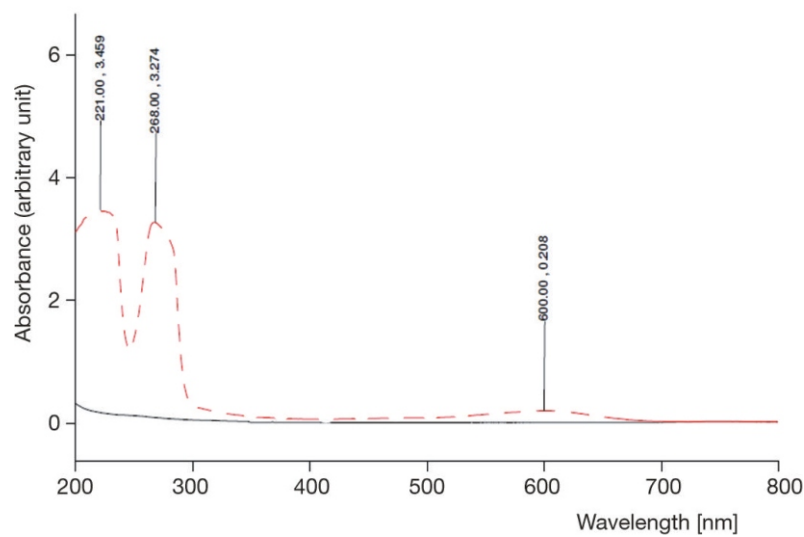


Figure 6. The UV-visible spectra of $^{99m}\text{Tc:MDA}$



Based on fig. 3, nine peaks were observed at 202 nm, 204 nm, 208 nm, 210 nm, 214 nm, 216 nm, 220 nm, 234 nm, and 357 nm. Transition peaks at 202-220 nm regions (dash line) show that the absorbance regions of ^{131}I with GO dropped by absorbing the UV rays in molecular excitations of the ^{131}I :GO compounds. Meanwhile, based on fig. 4, the maximum absorption peaks were observed to fall between the range of 200 nm to 360 nm, peaking at 203 nm, 234 nm, 238 nm, 242 nm, 246 nm, and 359 nm. The transition of a few single peaks within 203-359 nm regions (dash line) shows that the absorbance regions of $^{99\text{m}}\text{Tc}$ with GO dropped by absorbing the lower energies UV rays in molecular excitations compounds. Moreover, both absorbance spectra have many (fig. 3: 202 nm to 216 nm, fig. 4: 203 nm to 246 nm) peaks due to the electronic and vibrational transitions of the diatomic molecules that are present in the sample. Molecules can undergo both vibration and rotational motion, each of which results in energy changes. If the change is great enough, an electron in the molecule can pass to an excited quantum state [13]. Theoretically, peaks at 223 nm indicate that the sample contained a mixture of GO nanolayers [14].

The GO absorbance peak for ^{131}I decontaminated with GO was 220 nm (2nd dash line in fig. 3). However, the GO absorbance peak shifted to 234 nm (2nd dash line in fig. 4) for $^{99\text{m}}\text{Tc}$ decontaminated with GO. This was due to the additional oxygen between the layers of GO [11]. In addition, the highest absorption bands centred at 200 nm to 250 nm are explained by the π transition of aromatic C-C bonds, as shown in fig. 3 and fig. 4 [15]. The absorbance spectra for ^{131}I decontaminated with GO showed nine distinct peaks at 202 nm, 204 nm, 208 nm, 210 nm, 214 nm, 216 nm, 220 nm, 234 nm, and 357 nm. Meanwhile, for $^{99\text{m}}\text{Tc}$ decontaminated with GO, the absorbance spectra showed six peaks at 203 nm, 234 nm, 238 nm, 242 nm, 246 nm, and 359 nm. Peaks within the range of 200 nm to 250 nm are associated with the π transition [15]. The remaining peaks at 357 nm and 359 nm, as shown in fig. 3 and fig. 4, respectively, had not been observed. The peak at 361 nm was formed due to conjugated polyenes while in our case, the peaks were at 357 nm and 359 nm [14].

Based on fig. 5, five peaks were observed at 210 nm, 220 nm, 222 nm, 269 nm, and 608 nm. The absorbance varies between certain regions of high UV ray energies whereby the absorbance process gradually drops after 222 nm and regains at 269 nm (3rd dash line in fig. 5). This phenomenon might be due to energetic molecular electrons at the initial adsorption stage between ^{131}I :MDA. Meanwhile, in fig. 6, the maximum absorption peaks were observed to fall between the range of 200 nm to 600 nm, at 221 nm, 268 nm, and 600 nm. From the spectrum, the absorbance peaks obtained for $^{99\text{m}}\text{Tc}$:MDA were almost the same as ^{131}I :MDA in which there is a slope after 222 nm and re-

gain at 268 nm of UV regions (dash line in fig. 6). It is a saturation of radionuclide absorbance at certain regions by MDA and might be due to slow molecular interactions between the radionuclide elements with the functional groups of chemical compositions at molecular levels. Theoretically, the spectrum should have a broad peak as the molecules undergo an electronic transition as well as a vibrational and rotational transition [16]. This broad peak can be observed in both absorbance spectra of ^{131}I and $^{99\text{m}}\text{Tc}$ decontaminated with MDA due to the long absorbance process compared to GO nanolayers.

The GO characterisation

Figures 7 and 8 show the GO characterisation using FESEM to observe the surface morphology at

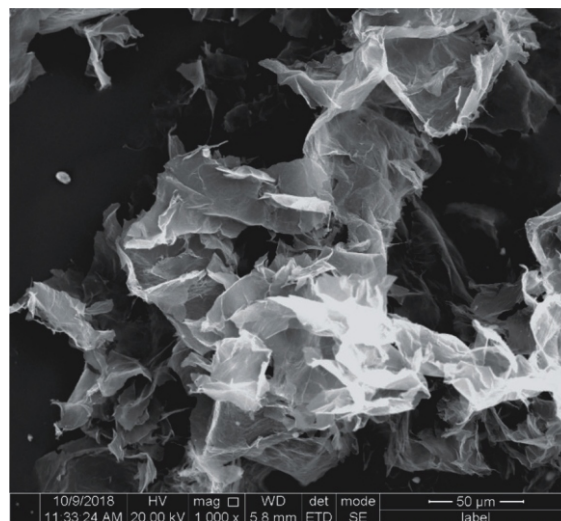


Figure 7. The FESEM image taken from GO at 1000 magnification shows wrinkle wax-tissue layers structures

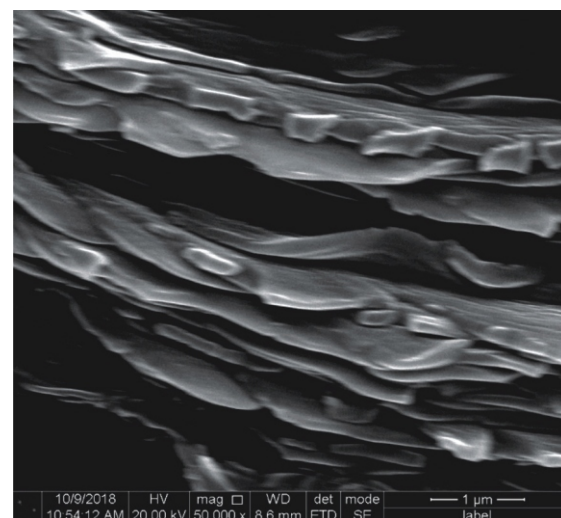


Figure 8. The FESEM image taken from GO at 50000 magnification shows folded continuous stacked nanolayers structures

different cross-sections. Figure 8 shows the 2-D geometry and individual sheets of GO in a random orientation. A randomly distributed, overlapped, thin layer of GO with a smooth surface, and a loosely stack-like morphology, can be visualised. Furthermore, the paper-like graphene with a continuous silk veil wave can be visualised, which contrasts sharply with the aggregated graphene produced by the chemical-based reduction of GO solution [17]. Some agglomeration and individual sheets are identifiable. Furthermore, a porous network structure like foam or a sponge can also be visualised. The porous network was formed due to the formation of large amounts of pores in the graphene nanostructures that created sponge-like graphene materials [18]. The morphology of a single GO sheet, as observed in fig. 7, looks like 'wax tissue layers' [19, 20]. This structure and layer-by-layer appearance at nano-size contributed to the high capacity for adsorption affinity [21]. The extensive surface area is also demonstrated on this single GO sheet, which contributes to the availability of additional functional groups and active sites [22]. Other than that, the GO surface also appears wrinkly like scrunched paper.

Based on fig. 8, a highly ordered structure of nano-sheet layers of GO, which look like abundant stacked wax-tissue layers, can be observed. These nano-sheet layers can be thought of as folded or continuous layers, and the margins of each sheet have kinked and wrinkled portions on the sides. Numerous layers can be stacked as a result of the chemical bond between the GO layers, which rapidly leads to aggregation [23]. The separation of layers is due to the oxygen functionalities on the graphene surface resulting from the oxidation process (the addition of oxygen lattice into the structures) in the preparation of GO, which consequently distorted the carbon lattice. The presence of oxygen functional groups on the graphene surface enhanced the separation of the layers and improved GO hydrophilicity. As a result, GO can be very easily dispersed in various media including aqueous and organic solvents [18]. The sponge-like porous network structure can be visualised clearly in fig. 8. The intercalation and removal of impurities between the graphene sheets, such as zinc oxide, will lead to the availability of pores in the graphene nanostructures and these features enable GO to act as a good absorbent [18].

CONCLUSION

The activity of ^{131}I after decontamination with MDA was slightly higher than the activity of ^{131}I decontaminated with the maximum concentration of GO, and these observations contradicted our expectations. This indicates that MDA is slightly more efficient than high concentrations of GO in the adsorption of ^{131}I . Meanwhile, the graph activity of $^{99\text{m}}\text{Tc}$ after de-

contamination decreased exponentially with higher concentrations of GO throughout the six hours, which corresponded to the expected results. When the concentration of GO increased, more $^{99\text{m}}\text{Tc}$ was trapped by the higher amounts of GO. Meanwhile, the $^{99\text{m}}\text{Tc}$ activity after decontamination with MDA was slightly lower than $^{99\text{m}}\text{Tc}$ decontaminated with the maximum concentration of GO. This shows that a high concentration of GO is more efficient than MDA in the adsorption of $^{99\text{m}}\text{Tc}$. The UV-Visible spectra for $^{99\text{m}}\text{Tc}$ and ^{131}I decontaminated with GO exhibited maximum absorption within the range of 200 nm to 250 nm, which was attributed to the π transition. Meanwhile, the absorbance spectra for $^{99\text{m}}\text{Tc}$ and ^{131}I decontaminated with MDA showed broad peaks indicating that MDA molecules undergo complex variations of electronic transition as well as vibrational and rotational transition. The transitions that were determined demonstrate that interaction changes happen during the adsorption process of $^{99\text{m}}\text{Tc}$ and ^{131}I . Overall, GO has a high potential to be proposed as an economical decontamination agent that is environmentally friendly with an achievable nuclear waste management sustainability for $^{99\text{m}}\text{Tc}$.

ACKNOWLEDGEMENTS

This work was supported by a Short-Term Research Grant from Universiti Sains Malaysia [304/PPSK/6315499]. We express our appreciation to Mr. Nik Fakurudin Nik Ali and Miss Wan Norhasikin Wan Marizam of the School of Health Sciences, University of Sains Malaysia for their help in obtaining the FESEM micrographs. Our appreciation goes to the Department of Nuclear Medicine, Radiotherapy & Oncology, Hospital University of Sains Malaysia for the use of their facilities when conducting the research.

AUTHORS' CONTRIBUTIONS

Original manuscript writing: M. K. A. A. Razab and R. Sunaiwi.

Data curation: R. Sunaiwi, F. H. Hadzuan and F. Ibrahim.

Supervision: M. K. A. A. Razab, N. M. Nawi, M. Z. A. Aziz, and A. T. Khaizul.

Data analysis: M. K. A. A. Razab and R. Sunaiwi.

Data validation: M. K. A. A. Razab, N. M. Nawi, N. H. Abdullah, and A. M. Noor.

Final revision: M. K. A. Abdul Razab, N. M. Nawi, N. Ha. Abdullah, A. M. Noor, and M. Z. A. Aziz.

REFERENCES

- [1] Nawi, N. M., *et al.*, Correlation of External Dose Rate with Whole Body Clearance Estimation in Radioiodine Therapy for rhTSH and THW Patients, *Journal of Radi-*

- ation Research and Applied Sciences, 13 (2020), 1, pp. 240-245
- [2] Akgun, E., *et al.*, Therapeutic Applications of Radiopharmaceuticals: An Overview, *Fabard Journal of Pharmaceutical Sciences*, 46 (2021), 1, pp. 93-104
- [3] ***, Opportunities and Approaches for Supplying Molybdenum-99 and Associated Medical Isotopes to Global Markets, The National Academies Press, Washington, 2018, pp. 1-8
- [4] ***, Technetium-99m, StatPearls, Treasure Island, 2021, pp. 1-13
- [5] Wong, K. K., *et al.*, Efficacy of Radioactive Iodine Treatment of Graves' Hyperthyroidism Using A Single Calculated ^{131}I dose, *Clinical Diabetes and Endocrinology*, 4 (2018), 20, pp. 1-8
- [6] Hussain, R. P., Management of Radioactive Spills in Nuclear Medicine; Teaching and Assessing with Objectively Structured Assessment of Technical Skills, *World Journal of Nuclear Medicine*, 14 (2015), 2, pp. 89-94.
- [7] Akchata, S., *et al.*, Influence of Decontaminating Agents and Swipe Materials on Laboratory Simulated Working Surfaces Wet Spilled with Sodium Pertechnetate, *Indian Journal of Nuclear Medicine*, 32 (2017), 3, pp. 173-176
- [8] Bomanji, J. B., *et al.*, Radiation Accidents and Their Management, *Nuclear Medicine Communications*, 35 (2014), 10, pp. 995-1002
- [9] Pecoraro, R., *et al.*, Toxicity Evaluation of Graphene Oxide and Titania Loaded Nafion Membranes in Zebrafish, *Frontiers in Physiology*, 8 (2018), 1039, pp. 1-7
- [10] Noor, A. M., *et al.*, Facile Preparation of Graphene Oxide Silver Aerogel for Antibacterial, *Journal of Tropical Resources and Sustainable Sciences*, 6 (2018), 1, pp. 41-44
- [11] Zin, F. A. M., *et al.*, Synthesis of Silver Graphene Oxide Nanocomposite Reinforced with Kenaf Cellulose Nanofibril Aerogel, *AIP Conference Proceedings*, 2068 (2019), 1, p. 020045
- [12] Noor, A. M., *et al.*, Laser Scribe Silver-Reduced Graphene Oxide as Novel Bactericidal Filter, *AIP Conference Proceedings*, 2068 (2019), 1, p. 020026
- [13] ***, Physical Chemistry, Oxford University Press, Great Britain, 2006, 481-512
- [14] Uran, S., *et al.*, Study of Ultraviolet-Visible Light Absorbance of Exfoliated Graphite forms, *AIP Advances*, 7 (2017), 3, p. 035323
- [15] ***, Organic Spectroscopy, Kluwer Academic Publishers, 2005, pp. 7-45
- [16] ***, Principles and Applications of Quantum Chemistry, Academic Press, 2016, pp. 291-337
- [17] Wang, H., *et al.*, Creation of Nanopores on Graphene Planes with MgO Template for Preparing High-Performance Supercapacitor Electrodes, *Nanoscale*, 6 (2014), 12, pp. 6577-6584
- [18] ***, Synthesis, Technology and Applications of Carbon Nanomaterials, Matthew Deans, 2019, pp. 77-107
- [19] Razab, M. K. A. A., *et al.*, Characterization of GO:I-131 for Radioactive Clinical Waste Water Management in Nuclear Medicine, *Material Science Forum*, 1010 (2020), pp. 561-566
- [20] Razab, M. K. A. A., *et al.*, Preliminary Study of the Potential Graphene Oxide as Radioactive Clinical Wastewater Adsorbability in Nuclear Medicine, *IOP Conference Series of Earth & Environmental Science*, 596 (2020), 012037, pp. 1-7
- [21] Jiričkova, A., *et al.*, Synthesis and Applications of Graphene Oxide, *Materials*, 15 (2022), 3, p. 920
- [22] Lu, S., *et al.*, Adsorption of Radionuclides on Carbon-based Nanomaterials, *Interface Science and Technology*, 29 (2019), pp. 141-215
- [23] Wei, B., *et al.*, Graphene Oxide Adsorption Enhanced by Attapulgite to Remove Pb (II) from Aqueous Solution, *Applied Sciences*, 9 (2019), 7, p. 1390

Received on June 3, 2022

Accepted on September 16, 2022

**Мохамад Хаирул Азхар Абдул РАЗАБ, Норазлина Мат НАВИ, Росидах СУНАИВИ,
Анамт Мохамед НУР, Мохд Захри Абдул АЗИЗ, Фара Нана Мохд ХАЏУАН,
Фатирах ИБРАХИМ, Ахмад Таифур ХАИЗУЛ, Нор Хакимин АБДУЛАХ**

ЕФИКАСНОСТ ТРЖИШНОГ СРЕДСТВА ЗА ДЕКОНТАМИНАЦИЈУ И ГРАФЕН ОКСИДА НА ИЗЛИВАЊЕ $^{99\text{m}}\text{Tc}$ И ^{131}I У ОДЕЉЕЊУ НУКЛЕАРНЕ МЕДИЦИНЕ

Рад са отвореним изворима радиоактивних супстанци у нуклеарној медицини је свакодневни задатак јер се контаминација услед изливања радиоактивних материјала може често десити. Правилно и безбедно управљање деконтаминацијом је витална процедура. Међутим, редовна куповина средстава за деконтаминацију носи високе трошкове и може бити токсична због својих хемијских својстава. Сврха овог рада је да упореди графен оксид, који је еколошки прихватљив материјал на бази угљеника са тржишним средством за деконтаминацију – при деконтаминацији радиоактивног изливања. Узорци чистог $^{99\text{m}}\text{Tc}$ и ^{131}I из лабораторије просути су на петријеву посуду. Проливање је одмах деконтанирано штапићем са средством за деконтаминацију који се продаје на тржишту и брисом графен оксида у различитим концентрацијама. Почетна радиоактивност сваког бриса који садржи $^{99\text{m}}\text{Tc}$ и ^{131}I мерена је коришћењем калибратора дозе. Спектри апсорбовања сваког узорка анализирани су коришћењем ултраљубичастог спектрофотометра. Морфолошка слика графен оксида посматрана је скенирајућим електронским микроскопом. За деконтаминацију коришћењем агенса за деконтаминацију који се продаје на тржишту, радиоактивност ^{131}I је била нешто већа, док је $^{99\text{m}}\text{Tc}$ била нешто нижа од високе концентрације графен оксида. Спектри апсорпције $^{99\text{m}}\text{Tc}$ и ^{131}I који су деконтанирани коришћењем графен оксида примећени су у опсегу од 200 nm до 250 nm услед * прелаза.

Кључне речи: нуклеарна медицина, радиоактивност, ^{131}I , $^{99\text{m}}\text{Tc}$, графен оксид, изливање, деконтаминација